#### **PAPER**

## Normal-state and superconducting properties of Co-doped BaFe<sub>2</sub>As<sub>2</sub> and MgB<sub>2</sub> thin films after focused helium ion beam irradiation

To cite this article: L Kasaei et al 2019 Supercond. Sci. Technol. 32 095009

View the article online for updates and enhancements.

#### Recent citations

- The role of the femtosecond laser induced nano/micro structures on the optical features of the steel surface; experimental polarimetry study

Morteza Asghari et al



### IOP ebooks™

Bringing together innovative digital publishing with leading authors from the global scientific community.

Start exploring the collection-download the first chapter of every title for free.

# Normal-state and superconducting properties of Co-doped BaFe<sub>2</sub>As<sub>2</sub> and MgB<sub>2</sub> thin films after focused helium ion beam irradiation

L Kasaei<sup>1</sup>, V Manichev<sup>2</sup>, M Li<sup>2</sup>, L C Feldman<sup>3,4</sup>, T Gustafsson<sup>3</sup>, Y Collantes<sup>5</sup>, E Hellstrom<sup>5</sup>, M Demir<sup>1</sup>, N Acharya<sup>1</sup>, P Bhattarai<sup>1</sup>, Ke Chen<sup>1</sup>, X X Xi<sup>1</sup> and B A Davidson<sup>1</sup>

E-mail: Leila.kasaei@temple.edu

Received 22 March 2019, revised 10 June 2019 Accepted for publication 27 June 2019 Published 1 August 2019



#### **Abstract**

We have investigated the normal-state and superconducting properties of Co-doped BaFe<sub>2</sub>As<sub>2</sub> (Ba122) and MgB<sub>2</sub> thin films irradiated at room temperature using a 30 keV focused He<sup>+</sup> ion beam with doses between  $10^{12}$  and  $10^{17}$  cm<sup>2</sup>. We show that superconductivity is suppressed and the normal-state resistivity is increased upon irradiation. The critical dose for the complete suppression of superconductivity is  $\sim 5 \times 10^{14}$  cm<sup>-2</sup> for Ba122 and  $\sim 8 \times 10^{15}$  cm<sup>-2</sup> for MgB<sub>2</sub>. The dependence of the normal-state and superconducting properties on irradiation dose is discussed, taking into account the spatial distribution of ion-induced damage. Hillock formation due to the substrate swelling, arising from the He<sup>+</sup> ions stopped in the substrate, is also observed. The findings provide guidelines for exploiting focused He<sup>+</sup> ion beam irradiation in fabricating iron pnictide and MgB<sub>2</sub> planar Josephson junctions.

Keywords: focused helium ion beam, ion-induced damage, superconductivity,  $MgB_2$ , Co-doped  $BaFe_2As_2$ 

1

(Some figures may appear in colour only in the online journal)

#### 1. Introduction

The Josephson effect in superconductors has been exploited in many analog and digital applications including superconducting quantum interference devices (SQUIDs), rapid single flux quantum (RSFQ) logic circuits, and Josephson voltage standards [1]. Developing a fabrication process capable of producing a large number of Josephson junctions uniformly

and reproducibly is crucial for using any superconductor materials, including the iron-based superconductors (FeSCs) and  $MgB_2$ . The most immediately obvious property of  $MgB_2$  which make it an ideal material for use in superconducting devices is the high critical temperature ( $T_c$ ) of 40 K which result in device operating temperature to be above 20 K. In addition, small penetration depth and multigap nature of  $MgB_2$  are beneficial in SQUID and RSFQ application. In the case of

<sup>&</sup>lt;sup>1</sup> Department of Physics, Temple University, Philadelphia, PA 19122, United States of America

<sup>&</sup>lt;sup>2</sup> Department of Chemistry and Chemical Biology, Rutgers University, Piscataway, NJ 08854, United States of America

<sup>&</sup>lt;sup>3</sup> Department of Physics and Astronomy, Rutgers University, Piscataway, NJ 08854, United States of America

<sup>&</sup>lt;sup>4</sup> Department of Materials Science and Engineering, Rutgers University, Piscataway, NJ 08854, United States of America

<sup>&</sup>lt;sup>5</sup> Applied Superconductivity Center, Florida State University, Tallahassee, FL 32310, United States of America

**Table 1.** Characteristics of the Co-doped Ba122 and MgB<sub>2</sub> thin films.

	Substrate	Growth technique	Critical temperature	Film thickness	Passivation layer	Passivation thickness
Co-doped Ba122	LSAT (001)	PLD	~17.9 K	50 nm	SiO <sub>2</sub>	7 nm
MgB <sub>2</sub>	SiC (0001)	HPCVD	~40 K	40 nm	MgO	7 nm

FeSCs, while ongoing effort to lay down the underlying mechanism for superconductivity continues, studying the Josephson effect could also provide a phase-sensitive measurement to reveal the symmetry of the superconducting order parameter, a fundamental question about the pnictide superconductors still not fully understood [2]. Besides, 122 compounds have small anisotropy and relatively high- $T_c$  opening the way for possible application. In spite of pioneer works on Josephson junctions and SQUID device using grain boundaries [3, 4] and heterojunctions [5, 6] of 122 family, achieving reproducible high-quality JJs remains a challenge.

To create a Josephson barrier in MgB<sub>2</sub>, a focused ion beam (FIB) has been used to either create a microbridge on a superconducting film or remove the material in a narrow gap on the film until only a very thin layer remains, thus forming a weak link barrier for Josephson junctions [7–9]. Sputtering of the superconductor by the ion beam is involved in this approach, and relatively heavy ions like gallium are usually used. However, this approach is prone to degradation of the superconductor/barrier interface, and it is difficult to reproducibly control the dimensions of the microbridge or the layer thickness in the gap. Another approach to fabricate Josephson junctions with FIB is direct writing without bulk sputtering of the material. Here, the FIB locally weakens or destroys the superconducting properties of the film to create a junction barrier. The effects of ion irradiation on the properties of various superconductors have been well documented, for example, in cuprates [10], iron-based pnictide superconductors [11], and MgB<sub>2</sub> [12, 13]. In a Josephson junction, the two superconductor films must be separated by only about a coherence length in order to achieve interference of the superconducting order parameters in the two superconductors. Heavy ions like gallium, with a FIB spot size of 5 nm, cannot be used to define a narrow junction barrier for superconductors with short coherence lengths. In contrast, the helium ion microscope (HIM) creates a beam of light He<sup>+</sup> ions and can deliver a focused beam with a diameter of less than 0.5 nm, comparable to the short coherence lengths in hightemperature cuprate superconductors and iron-based pnictides. Nano Josephson tunnel junctions in YBa<sub>2</sub>Cu<sub>3</sub>O<sub>7</sub> by using the focused helium ion beam have been successfully demonstrated [14, 15]. The short coherence length of  $\sim 2.5 \, \mathrm{nm}$  of BaFe<sub>1.84</sub>Co<sub>0.16</sub>As<sub>2</sub> (Co-doped Ba122) [16] also demands a narrow barrier region to permit Josephson coupling, making the direct writing with a focused He<sup>+</sup> ion beam a promising path for fabricating pnictide Josephson junctions.

To fabricate Ba122 and  $MgB_2$  Josephson junctions with a focused  $He^+$  ion beam, one needs to understand the irradiation effects on both the normal-state and the superconducting properties of these materials. This information has not been reported to date. The most relevant results are on

200 keV proton irradiation of Ba122 films [17] and on 2 MeV  $^4$ He $^{++}$  ion irradiation of MgB $_2$  films [18]. A FIB was not used in these studies. In both works, although the transition temperature  $T_c$  was found to decrease upon irradiation, complete suppression of superconductivity was not found up to the highest dose used. In this paper, we report on the modification of the normal-state resistivity and superconducting transition temperature of Co-doped Ba122 and MgB $_2$  thin films by 30 keV focused He $^+$  ion beam irradiation. In both cases, complete suppression of  $T_c$  was observed. The systematic changes in  $T_c$  and resistivity provide guidelines for using a focused He $^+$  ion beam to fabricate planar Ba122 and MgB $_2$  Josephson junctions.

#### 2. Experimental details

Epitaxial thin films of optimally doped Ba122 were grown by pulsed laser deposition on  $5 \text{ mm} \times 5 \text{ mm}$  (001) (La, Sr)(Al, Ta)O<sub>3</sub> (LSAT) substrates at 730 °C [19]. The film thickness was 50 nm and exhibited zero-resistance at  $T_c \sim 17.9 \, \text{K}$ . A 20-nm protective Au layer was deposited in situ on the film at 200 °C. 40 nm thick MgB<sub>2</sub> films on 6 mm  $\times$  6 mm (0001) SiC substrates were grown by using hybrid physical-chemical deposition, as described elsewhere [20]. The as-grown films were immediately transferred to a DC magnetron sputtering chamber where a bilayer of Cr/Au (5 nm/20 nm) was sputtered on the films for protection during processing. Standard UV lithography and Ar ion milling were used to pattern a 4 or 5  $\mu$ m wide bridge on the films. Subsequently, a 300 nm thick Au film was sputter-coated on the contact pads, and the Au (Cr/Au) on top of the Ba122 (MgB<sub>2</sub>) bridge was removed by Ar ion milling. The entire sample was passivated with a 7 nm SiO<sub>2</sub> (by RF magnetron sputtering) in Ba122 and 7 nm MgO (by reactive DC magnetron sputtering of Mg target in an Ar/O<sub>2</sub> mixture) in MgB<sub>2</sub> (see table 1).

Focused He<sup>+</sup> ion beam irradiation was conducted at room temperature using a Zeiss Orion Plus HIM with a 30 keV He<sup>+</sup> beam with a ~0.5 nm spot size. The beam was perpendicular to the plane of the film; thus the possibility of channeling through the crystal cannot be excluded. Transport of ions in matter (TRIM) computer code [21] was used to simulate the interactions of the He<sup>+</sup> ions in the film/substrate geometry. Figure 1(a) shows the resulting distribution of 30 keV He<sup>+</sup> ion range in a 7 nm SiO<sub>2</sub>/50 nm Ba122/LSAT substrate sample. The thickness of the Ba122 film was chosen to be much smaller than the range of the He<sup>+</sup> ions, which therefore nearly completely penetrate the film into the substrate. The same consideration was taken into account in choosing the thickness of the MgB<sub>2</sub> film.

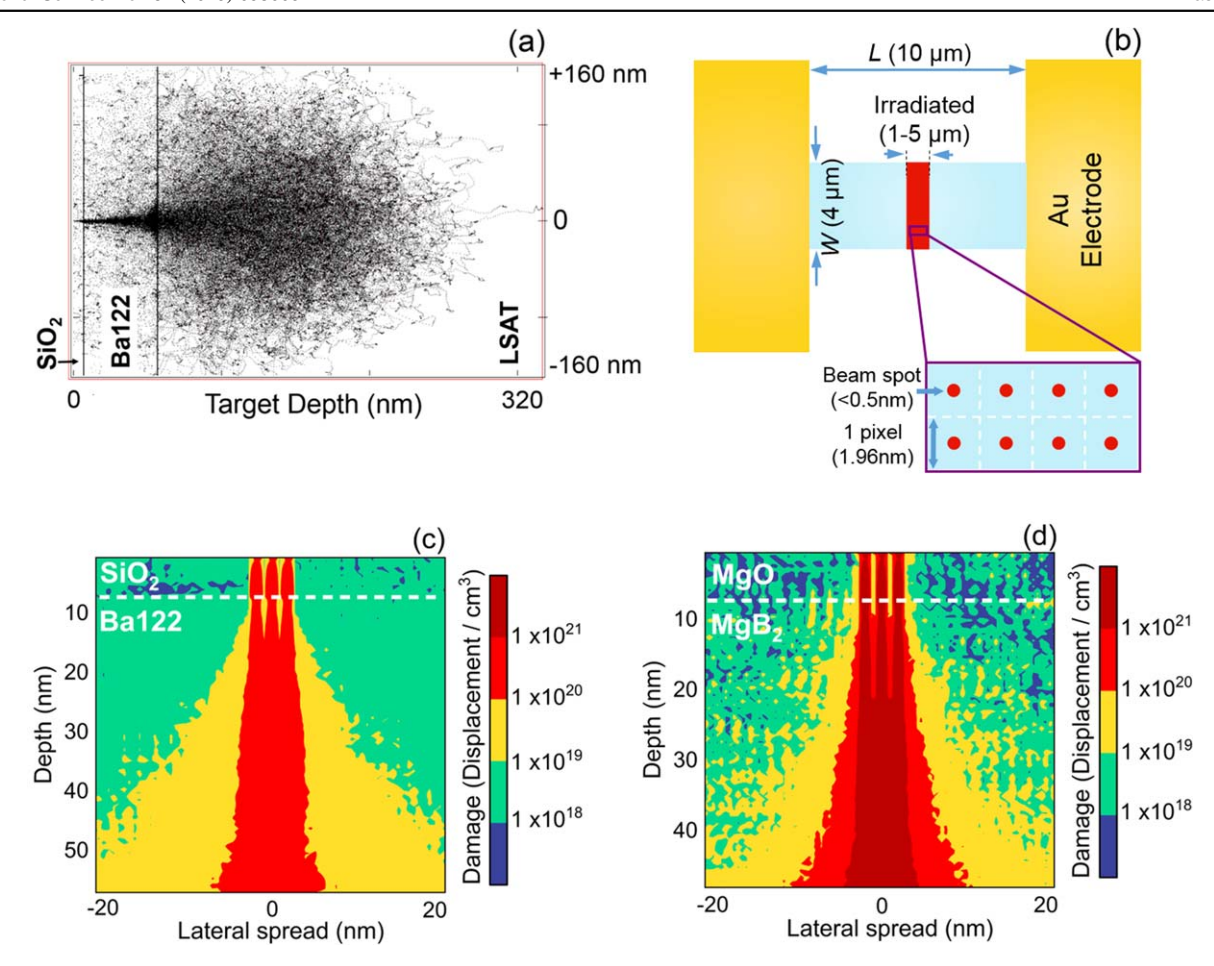


Figure 1. (a) TRIM simulation of the range of 30 keV He $^+$  ions in a 7 nm SiO $_2/50$  nm Ba122/LSAT sample. (b) Schematic of the sample with a 4  $\mu$ m  $\times$  10  $\mu$ m bridge. The blue area represents the pristine film. The focused He $^+$  ion beam was rastered over the red rectangle. The blowup of the irradiated area shows the raster pattern of the focused He $^+$  ion beam. The white dashed lines are guide to eye, showing a pixel size of 1.96 nm  $\times$  1.96 nm at the 100 nm FOV (c) TRIM simulation of the damage density profile for three adjacent single tracks of He $^+$  in the SiO $_2/B$ a122 sample at 5  $\times$  10<sup>14</sup> cm $^{-2}$  (d) TRIM simulation of the damage density profile for three adjacent single tracks of He $^+$  in the MgO/MgB $_2$  sample at 8  $\times$  10<sup>15</sup> cm $^{-2}$ .

To characterize the damage caused by the helium ion beam in the MgB<sub>2</sub> thin film, transmission electron microscope (TEM) measurements were performed using a JEOL JEM-2100 microscope operated at 200 kV. The sample was a 25 nm thick MgB<sub>2</sub> film/10 nm MgO passivation layer with a patterned 4  $\mu$ m × 10  $\mu$ m bridge, across which 4 single-pixel-width lines were irradiated with the focused helium ion beam at 4 different doses—8 × 10<sup>15</sup>, 2 × 10<sup>16</sup>, 6 × 10<sup>16</sup>, and 5 × 10<sup>17</sup> cm<sup>-2</sup>. To avoid cross-line dosing between adjacent lines [22], they were separated by 1.5  $\mu$ m distance. The cross-sectional TEM sample was prepared using a Dual Beam FIB-SEM (FEI Strata DB235).

For measuring the irradiation effects on  $T_c$  and the normal-state resistance, we rastered the He<sup>+</sup> beam to irradiate multiple tracks over a length of 1  $\mu$ m or 5  $\mu$ m in a 10  $\mu$ m long bridge. The geometry of the bridge and the irradiated area are illustrated in figure 1(b). The blowup of an irradiated area shows that, at a 100  $\mu$ m field of view (FOV), the pixel size is 1.96 nm  $\times$  1.96 nm, larger than the beam spot. The He<sup>+</sup> ion beam moved from the center of one pixel to the next, delivering the needed dose at each center spot. Figures 1(c) and (d) shows the simulated damage profile of three adjacent tracks caused by the He<sup>+</sup> ion irradiation in three beam spots, with 1.96 nm pixel spacing,

penetrating the  $SiO_2/Ba122$  and  $MgO/MgB_2$  film, respectively. Although the lateral spreading of the damaged regions quickly exceeds the beam spot size after the ions enter the film, overlapping over the entire irradiated area, the damage is not laterally uniform in the top part of the samples. Note that every single track is based on the simulation of 100k ions.

Electrical transport measurements over the bridges were performed by the four-point method. The total resistance,  $R_{\rm tot}$ , of the bridge can be modeled by three resistors in series,  $R_{\rm tot} = R_1 + R_2 + R_3$ , where  $R_2$  represents the resistance of the area irradiated by the ion beam and  $R_1$  and  $R_3$  are contributions from the unirradiated areas. The results for different irradiation doses were obtained from different bridges on the same sample or from different samples.

#### 3. Results and discussions

#### 3.1. Helium ion-induced damage in MgB2 thin film

Figures 2(a)–(d) show cross-sectional bright field (BF) TEM images of irradiated regions of four beam spots with doses of

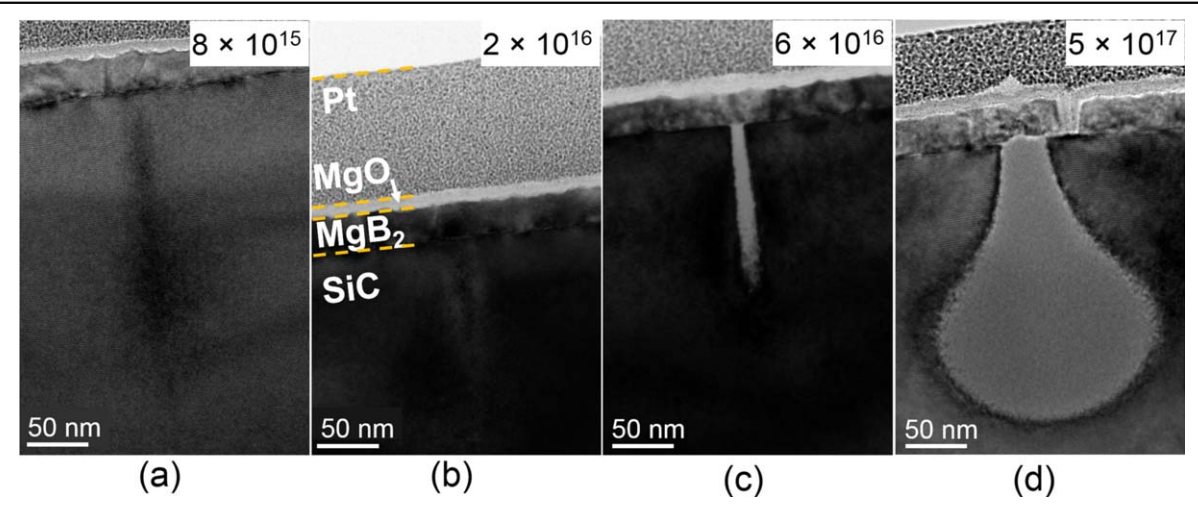
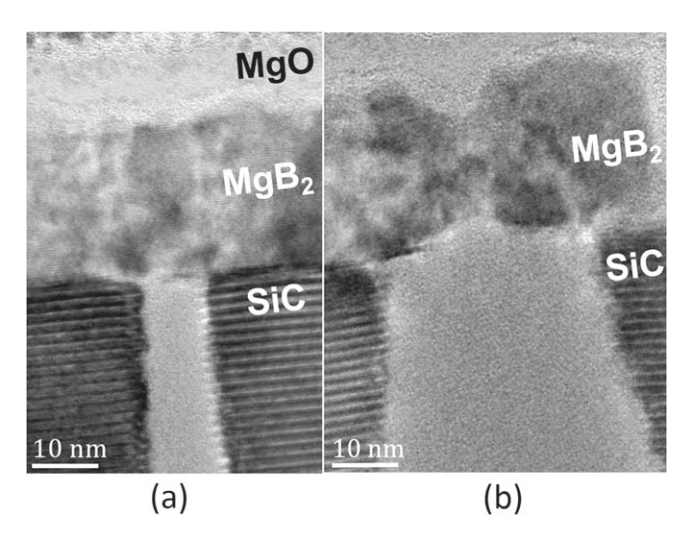


Figure 2. Complete series of BF TEM micrographs of thin film of (10 nm MgO/ 25 nm MgB<sub>2</sub>/on SiC substrate) irradiated by a 30 keV He<sup>+</sup> ion beam with increasing doses. The dose values on each micrograph are in ions cm<sup>-2</sup>.



**Figure 3.** TEM micrographs of the thin film of 10 nm MgO/ 25 nm MgB<sub>2</sub>/on SiC substrate irradiated with a helium ion dose of (a)  $6 \times 10^{16}$  cm<sup>-2</sup>, (b)  $5 \times 10^{17}$  cm<sup>-2</sup>.

 $8 \times 10^{15}$ ,  $2 \times 10^{16}$ ,  $6 \times 10^{16}$ , and  $5 \times 10^{17} \, \text{cm}^{-2}$ , respectively. While the damage is not visible in the MgB<sub>2</sub> film, it can be observed in the SiC substrate. At the two lowest doses, different contrasts in the irradiated regions in the substrate can be seen (figures 2(a) and (b)). At a dose of  $6 \times 10^{16} \, \text{cm}^{-2}$ , an amorphized region in the substrate is clearly visible (figure 2(c)). For the dose of  $5 \times 10^{17} \, \text{cm}^{-2}$ , the amorphous region in the substrate grows through the depth of the sample as well as laterally, as the damage produced by the ion beam also reaches the damage threshold to be visible (figure 2(d)). From figure 3, we find that the diameter of the amorphous region at the MgB<sub>2</sub>/SiC interface is  $\sim 10 \, \text{nm}$  for  $6 \times 10^{16} \, \text{cm}^{-2}$  and  $\sim 30 \, \text{nm}$  for  $5 \times 10^{17} \, \text{cm}^{-2}$ .

The amorphized region in the substrate observed in figure 2(d) is qualitatively consistent with the TRIM simulation. A quantitative one-to-one correspondence to the region where superconductivity is completely suppressed by ion irradiation is difficult to extract from these data, as the damage may be annealed during the electron microscope

measurement. We have observed such annealing effects in the low-dose samples. Nevertheless, we can conclude from the results that the region damaged by the He ion irradiation spreads much wider than the focused beam size when the ions travel deep into the film. The TRIM results in figures 1(c) and (d) provide a good guideline when we consider the irradiation effects on transport and superconducting properties of the superconductor films.

#### 3.2. Co-doped Ba122

Figure 4(a) shows electrical resistance versus temperature of four bridges on a Ba122 film, three of which were irradiated with different He<sup>+</sup> ion doses. At a dose of  $2 \times 10^{14}$  cm<sup>-2</sup>, a second transition with a lower transition temperature of 7.7 K and a residual resistance of 9.2  $\Omega$  appears, that correspond to the properties of the irradiated area. We denote the transition temperature of the irradiated region as  $T_c'$ , and the resistance above  $T_c'$  as  $R_2$ , schematically shown in figure 1(b). The properties of the unirradiated area remain unchanged, with an original transition temperature  $T_c$  of 17.9 K. At a dose of  $1 \times 10^{15}$  cm<sup>-2</sup>, the superconductivity in the irradiated area has been completely suppressed, and no zero resistance region is observed down to the lowest temperature measured. Further irradiation results in an additional increase in the resistivity of the irradiated area.

The transition temperature of the irradiated region normalized to that of the unirradiated region,  $T_c'/T_c$  is plotted against the He<sup>+</sup> ion dose in figure 4(b). The data points were collected from multiple bridges and multiple samples and the midpoint of the higher-temperature transition taken as  $T_c$ . Therefore, a normalization to the unirradiated  $T_c$  was necessary to make the data comparable.  $T_c'$  decreases with increasing irradiation dose, and superconductivity is completely suppressed at a critical dose of  $5 \times 10^{14} \, \mathrm{cm}^{-2}$ . Figure 4(c) shows TRIM simulation for vacancy concentrations for As, Ba, and Fe, as well as total vacancy concentration produced by this dose of He<sup>+</sup> ions as a function of depth from the sample surface. Below the surface, this

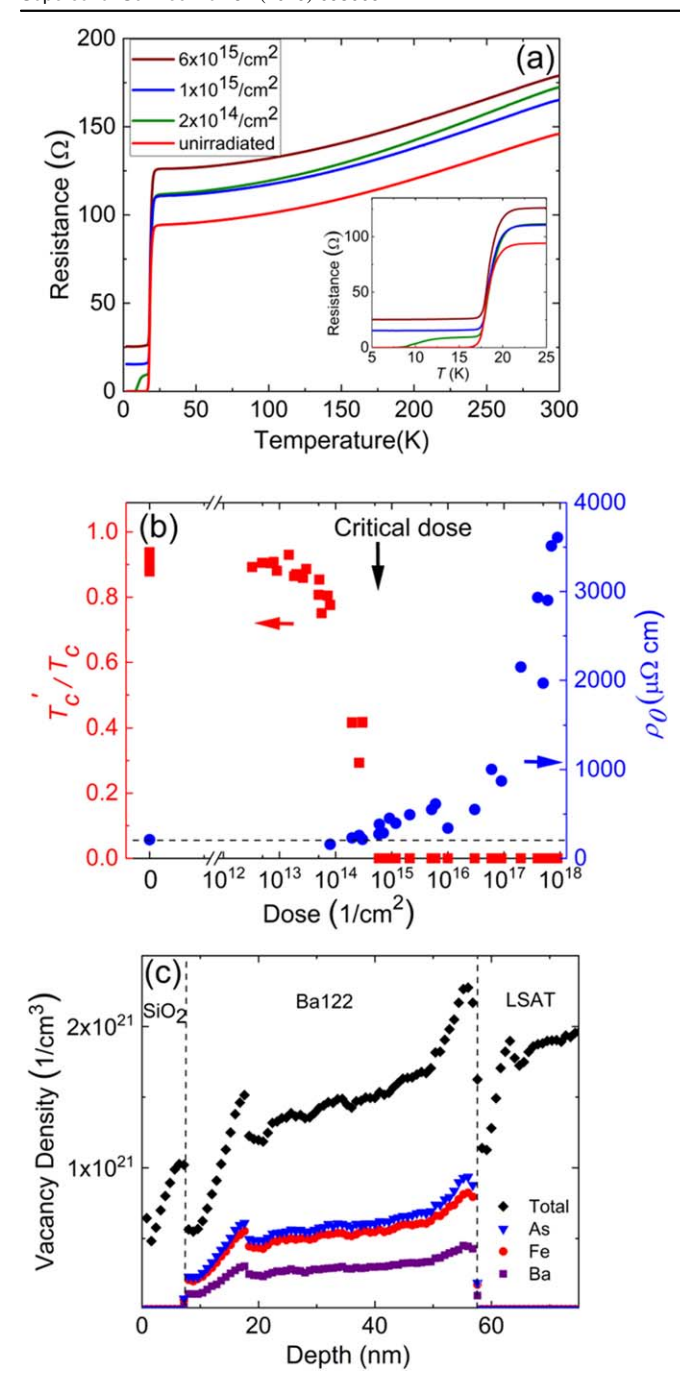


**Figure 4.** (a) Resistance versus temperature curves for four Ba122 bridges irradiated at different doses. The inset shows details near the superconducting transition. (b) Normalized critical temperature  $T_c'/T_c$  and residual resistivity  $\rho_0$  of the irradiated region as functions of He<sup>+</sup> ion dose. Horizontal dashed line was drawn at the zero-dose resistivity. (c) Vacancy concentration for SiO<sub>2</sub>/Ba122/LSAT configuration at dose  $5 \times 10^{14} \, \mathrm{cm}^{-2}$  obtained from TRIM simulation.

concentration is higher than seen in figure 1(c) because of overlapping profiles of many pixels. Near the film surface, the damage regions from the adjacent pixels do not overlap, and the vacancy concentration results are not reliable. At depths greater than 20 nm, the total vacancy concentration is of the order 10<sup>21</sup>/cm<sup>3</sup>, increasing gradually towards the film/substrate interface. This is a very high vacancy concentration,

about 2% of all atoms. It is possible that the top layer of the films, where the damaged regions from the adjacent beam spots do not overlap, retains a continuous superconducting path until a much higher dose when superconductivity in the outermost area is suppressed. This implies that the measured critical dose indicated in figure 4(b) is an upper limit to the critical dose in ideally uniform irradiation conditions. In the 200 keV proton irradiation experiment reported in [17], the highest dose,  $1.8 \times 10^{15}\, \text{cm}^{-2}$ , created a vacancy concentration of the order 10<sup>20</sup>/cm<sup>3</sup>, but complete suppression of  $T_c$  was not achieved. Combined with optical conductivity measurement, Schilling et al suggested that proton irradiation-induced disorder causes a closing and reopening of the superconducting gap on one of the Fermi surface sheets, accompanied by a sign change, thus changing the order parameter symmetry from  $s_{\pm}$  to  $s_{++}$  [17]. This explanation, however, needs to be reconciled with the complete suppression of superconductivity reported in this work.

Also plotted in figure 4(b) is the residual resistivity  $\rho_0$ , calculated using the nominal area of the irradiated region. The residual resistivity of the unirradiated Ba122 films is around  $100 \,\mu\Omega$  cm. Upon He<sup>+</sup> ion irradiation, the resistivity dips below the unirradiated value at doses less than the critical dose, then monotonically increases to about  $1000 \mu\Omega$  cm at around 10<sup>17</sup> cm<sup>-2</sup>, followed by a sharp upturn at higher doses. The behavior of  $T'_c$  and  $\rho_0$  shown in figure 4(b) is similar to that observed in  $YBa_2Cu_3O_{7-\delta}$  films irradiated with 75 keV He<sup>+</sup> ions, although the critical dose is six times lower for Ba122 than for YBa<sub>2</sub>Cu<sub>3</sub>O<sub>7- $\delta$ </sub> (3 × 10<sup>15</sup> cm<sup>-2</sup>) [23]. The wide range of irradiation doses between the disappearance of superconductivity and the rapid increase in the resistivity provides a tool to tune the properties of planar superconductor/normal metal/superconductor (SNS) in Ba122 using a focused He<sup>+</sup> ion beam.

#### 3.3. MgB<sub>2</sub>

Figure 5(a) shows the electrical resistance as a function of temperature for four bridges on an MgB2 film, three of which were irradiated with different He<sup>+</sup> ion doses. Similar to the overall trend in Ba122,  $T_c'$  decreases and resistivity increases when MgB2 is irradiated. However, the superconducting transition of the irradiated area persists to much higher irradiation doses than in Ba122: only when irradiated with close to  $10^{16} \,\mathrm{cm^{-2}\ He^{+}}$  ions is the superconductivity completely suppressed in the MgB<sub>2</sub> film. In figure 5(b),  $T_c'/T_c$  and  $\rho_0$  are plotted as functions of the He ion irradiation dose. A critical dose of  $8\times10^{15}\,\mathrm{cm}^{-2}$  for suppressing superconductivity is observed. Again, this dose may correspond to the value when the continuous superconducting path is completely destroyed in the top layer of the films, where the damaged regions from the adjacent beam spots do not overlap. It represents, as in the Ba122 case, an upper limit on the dose necessary to suppress superconductivity. Figure 5(c) TRIM simulation for vacancy concentrations in Mg, and B, as well as total vacancy concentration produced by  $8 \times 10^{15} \,\mathrm{cm}^{-2} \,\mathrm{He}^{+}$  ion dose as a function of depth from the sample surface. The total vacancy concentration at depths greater than 20 nm is of the order

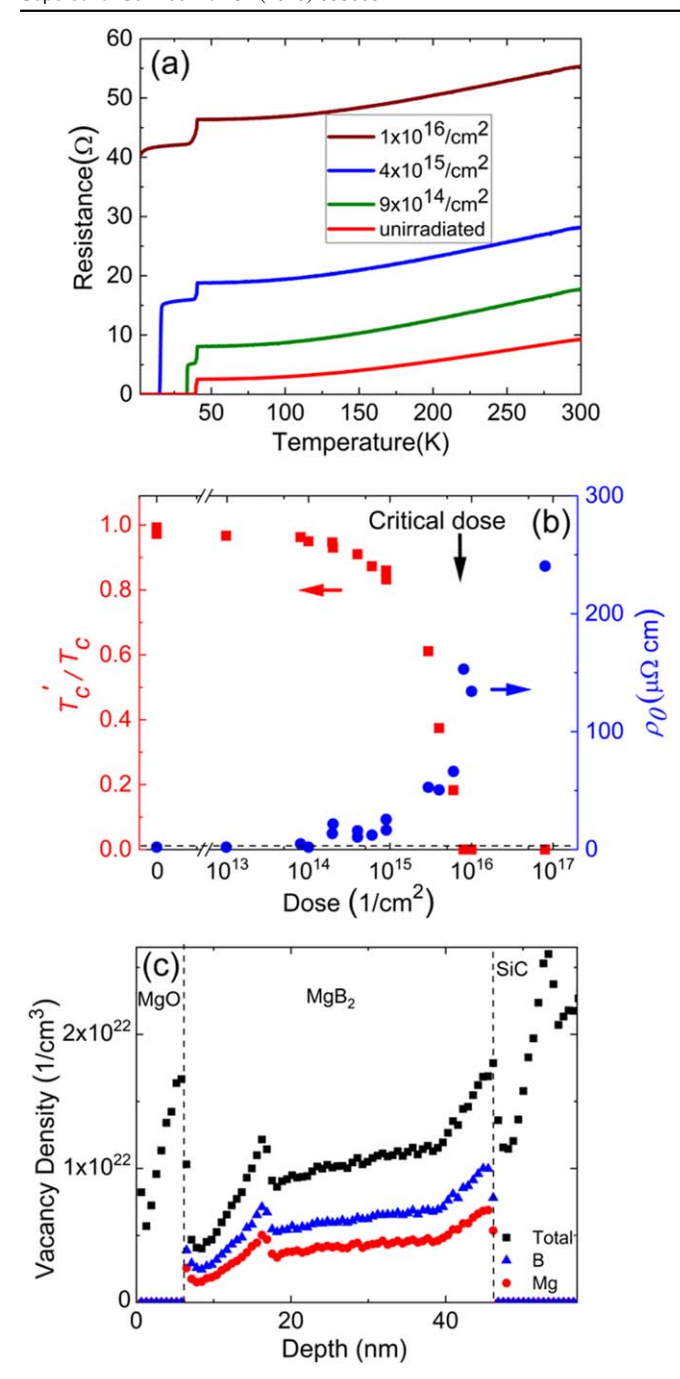


**Figure 5.** (a) Resistance versus temperature measurement for four MgB<sub>2</sub> bridges irradiated at difference doses. (b) Normalized critical temperature  $T_c'/T_c$  and residual resistivity  $\rho_0$  of the irradiated region as functions of the He<sup>+</sup> ion dose. Horizontal dashed line was drawn at the zero-dose resistivity. (c) Vacancy concentration for MgO/MgB<sub>2</sub>/SiC configuration at dose  $8 \times 10^{15} \, \mathrm{cm}^{-2}$  obtained from TRIM simulation.

 $10^{22}/\mathrm{cm}^3$ , and it increases slightly towards the film/substrate interface. This is a very high vacancy concentration, about 10% of all atoms, much higher than that produced by  $1.3\times10^{17}\,\mathrm{cm}^{-2}$  2 MeV  $^4\mathrm{He}^{++}$  ions irradiation  $(0.2\times10^{22}/\mathrm{cm}^3)$ , reported in [12], where no complete  $T_c$  suppression was observed. As mentioned above the TRIM results do not take into account channeling effects which can strongly modify/reduce defect creation. Such damage estimates

therefore might be high by as much as a factor of 10! The lack of complete  $T_c$  suppression in [12] may also be due to the high energy of the He<sup>+</sup> ions that generates an even lower concentration of vacancies near the film surface that could short out the more disordered part of the film. Unlike Ba122, for which resistivity increases only moderately when the superconductivity is suppressed, the resistivity of the irradiated MgB<sub>2</sub> has increased by 65 times at the critical dose. However, because the residual resistivity of the unirradiated MgB<sub>2</sub> film is low, about 2  $\mu\Omega$  cm, even after a nearly 100 times increase at an irradiation dose of  $10^{17}$  cm<sup>-2</sup>, it is still relatively low and the film maintains a metallic behavior. Thus, we expect planar Josephson junctions of MgB<sub>2</sub> made by focused He<sup>+</sup> ion beam irradiation to be SNS in nature [24, 25].

#### 3.4. Hillock formation

It is known that when irradiated with low-mass accelerated ions, swelling occurs in the crystalline substrate [26-29]. The cavity (bubble) formation has been linked to the mechanical properties of the target material [30]. This effect needs to be taken into account in considering the influence of focused He<sup>+</sup> ion beam irradiation on the properties of the pnictide and MgB<sub>2</sub> bridges. Figure 6(a) shows an atomic force microscope (AFM) image of a multiple-track irradiation at a He<sup>+</sup> ion dose of  $3 \times 10^{16} \,\mathrm{cm}^{-2}$  in which the irradiated area is elevated from the unirradiated area, clearly indicating hillock formation. The hillock was confirmed by a line scan along the blue line in the figure and shown below the AFM image. A nearly flat-topped hillock across the 5  $\mu$ m irradiated length with a height of around 27 nm was observed at this dose for the Ba122 film on LSAT substrate. For fabricating Josephson junctions with a single pixel line of focused He<sup>+</sup> ion beam irradiation, the hillock of a single track is the most relevant. An AFM image of a single-track irradiated Ba122 bridge and a line scan across the track are shown in figure 6(b). For a  $\mathrm{He^+}$  ion dose of  $4 \times 10^{17}\,\mathrm{cm^{-2}}$ , a hillock with a width of  $\sim$ 500 nm and a height of  $\sim$ 28 nm is seen in the figure. Similar hillocks for multiple-track and single-track irradiation have been observed in MgB<sub>2</sub> bridges on the SiC substrate. The width of the single-track hillock is about 1000 times larger than the ion beam spot. As shown in figure 1(a), the He ions stop deep inside the substrate and spread out to over a region with a  $\sim$ 300 nm diameter. Density change of material due to amorphization, and to a lesser extent, buried He<sup>+</sup> ions are responsible for the swelling of the substrate.

Figure 7 shows the hillock height as a function of He<sup>+</sup> ion dose for multiple-track and single-track irradiation on both Ba122 and MgB<sub>2</sub> bridges as well as on the bare LSAT and SiC substrates. In all cases, the hillock heights on the bridges are the same as on the bare substrates, confirming that the hillock formation is due to the swelling of the substrate [31]. The figure also shows that the swelling in SiC occurs at much lower doses than in LSAT, although the increase of the hillock height with irradiation dose is much slower. Single-track irradiation requires an order of magnitude more dose to generate hillocks of comparable height than the multiple-track

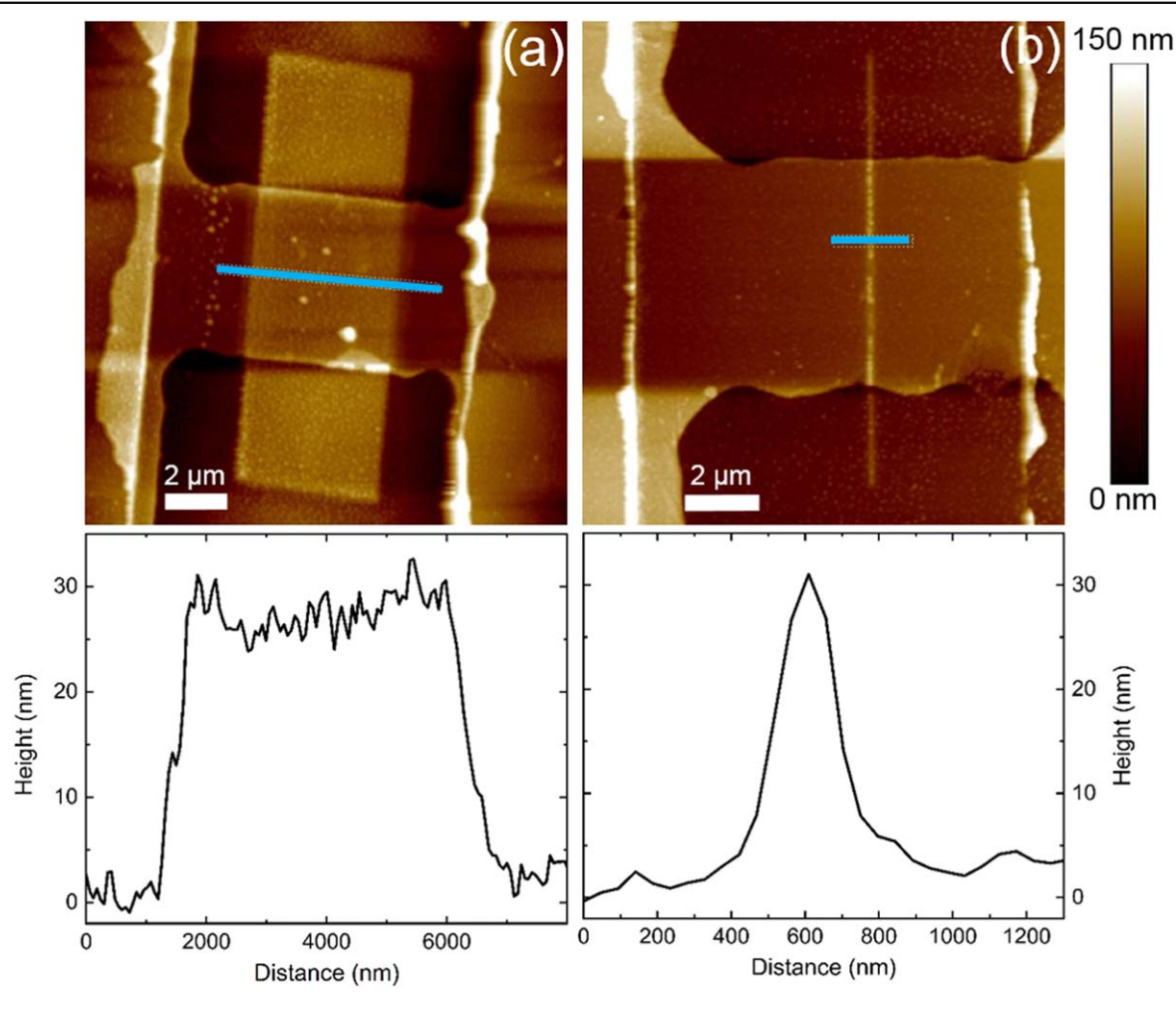


**Figure 6.** AFM images and line scans for (a) a multiple-track irradiated Ba122 bridge with a helium ion dose of  $3 \times 10^{16}$  cm<sup>-2</sup> and (b) a single-track irradiated Ba122 bridge with a helium ion dose of  $4 \times 10^{17}$  cm<sup>-2</sup>. The line scans are along the blue lines in the AFM images.

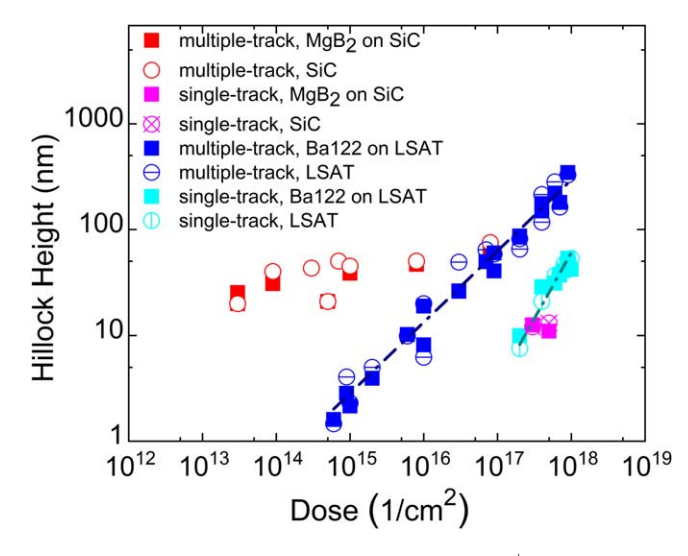


**Figure 7.** Hillock height as a function of He<sup>+</sup> ion dose.

irradiation, presumably because it is easier for the He ions to diffuse to the surrounding volume than in the case of multiple-track irradiation.

There does not seem to be a clear correlation between the suppression of superconductivity and hillock formation. In the case of Ba122, superconductivity is suppressed before the irradiation dose at which substantial hillock formation occurs. For MgB<sub>2</sub>, the hillock height does not change significantly around the critical dose. On the other hand, the hillock height does seem to be responsible for the upturn of residual resistivity of the Ba122 bridges. Above the dose where the upturn takes place, around  $10^{17}$  cm<sup>-2</sup>, the hillock height exceeds the Ba122 film thickness, creating steps at the edges of the irradiated region and leading to insulating behavior of the bridge resistivity below  $T_c$  (not shown). We cannot distinguish whether the insulating properties at such high doses are due to the hillock edges or are intrinsic to the heavily irradiated film.

#### 3.5. Nature of defects produced by 30 keV He<sup>+</sup> irradiation

The nearly rigid vertical shift in the  $\rho(T)$  curves as a function of dose in figures 4(a) and 5(a) implies that irradiation increases impurity scattering, leaving the carrier concentration unchanged. Disorder has been proposed as a probe of order parameter symmetry in a two-band superconductor like Ba122 since complete suppression of superconductivity at relatively low levels of disorder suggesting that impurity scattering is pair-breaking, as would only occur in scattering between bands of opposite signs e.g. in the case of  $s_{\pm}$  order

parameter symmetry [32]. A quantitative treatment of  $T_c$ suppression versus impurity scattering rate requires knowledge of the ratio of intra- to interband scattering rates [33], which becomes a free parameter when fitting the experimental data within the Abrikosov-Gor'kov theory [34]. For pointlike defects that occur under electron irradiation of Ru-substituted Ba122, complete suppression of  $T_c$  would be observed for a change in residual resistivity  $\rho_0 \approx 40~\mu\Omega$  cm, yielding a ratio of 0.65 for the scattering rates [35]. In comparison,  $\alpha$ -particle irradiation is not typically expected to produce point-like defects though there is some evidence that this can also be the case [17]. For irradiation with 30 keV He<sup>+</sup> ions, a closer analysis of the data in figure 4(b) show that in these experiments complete suppression of  $T_c$  occurs around  $\rho_0 \approx 20~\mu\Omega$  cm. Assuming the same considerations as those in [35], the data presented here indicates a scattering ratio closer to 1. We note that this is most likely an overestimate since our resistivity data is likely underestimated due to the nonuniformity of the displacement densities mentioned earlier and shown in figure 1(c). Nevertheless, these estimates are reasonable and offer additional support for  $s_{\pm}$  over  $s_{++}$ symmetry. Further investigation of this approach to study  $T_c$ suppression would require improving the uniformity of irradiation-induced displacements, in principle possible with the HIM used here.

#### 4. Conclusions

Focused He<sup>+</sup> ion beam irradiation is shown to completely suppress superconductivity in Ba122 and MgB2 thin films. The critical dose required to suppress superconductivity is  $\sim 5 \times 10^{14} \, \text{cm}^{-2}$  for Ba122 and  $\sim 8 \times 10^{15} \, \text{cm}^{-2}$  for MgB<sub>2</sub>, corresponding to large vacancy concentrations in the films. In the case of Ba122, the normal-state resistivity experiences large increases above the critical dose and becomes insulating when hillock height exceeds the film thickness. In contrast, even with increases of 100 times at high irradiation dose, MgB<sub>2</sub> maintains a metallic behavior with low resistivity. In either case, the focused He<sup>+</sup> ion beam process is suitable for creating planar SNS junctions. It should be noted that the irradiation-induced disorder spreads out beyond the focused ion spot size in the depth of the film as shown in figures 1(c), (d). Thus, in fabricating a Josephson junction with a focused He<sup>+</sup> ion beam, one should minimize the thickness of the film so that the damaged area remains narrow enough for the interference of the order parameter to take place. It should also be noted that when irradiating multiple-tracks, the damage density throughout film might not be uniform as there may be a layer near the first interface where the damaged regions do not overlap. Also, the specific values of the irradiation doses for suppression of superconductivity and increase of resistivity presented here are for the multiple-track irradiation and may differ from those in the single-track irradiation. Nevertheless, the results are useful to guide the development of a focused He<sup>+</sup> ion beam technology for fabricating iron pnictide and MgB<sub>2</sub> planar Josephson junctions. Indeed, MgB2 Josephson junctions have been produced by focused He<sup>+</sup> ion beam irradiation with single-track irradiation with doses of  $9 \times 10^{15} \, \mathrm{cm}^{-2}$  and  $2 \times 10^{16} \, \mathrm{cm}^{-2}$  [24], close to the critical dose of MgB<sub>2</sub>. The complete suppression of superconductivity in Ba122 by irradiation also sets constraints for theoretical models on the disorder-induced change of order parameter symmetry in Ba122 from  $s_{\pm}$  to  $s_{++}$  [17].

#### **Acknowledgments**

This material is based upon work supported by the National Science Foundation under Grant No. DMR-1310087. We acknowledge the use of services and facilities of Temple Materials Institute at Temple University. Work done at Florida State University was supported by NSF-DMR 1306785, within the National High Magnetic Field Laboratory, which is supported by the National Science Foundation Cooperative Agreement No. DMR-1157490, and the State of Florida.

#### **ORCID iDs**

L Kasaei https://orcid.org/0000-0003-2560-8074

#### References

- [1] Gross R, Marx A and Deppe F 2015 Applied
  Superconductivity: Josephson Effect and Superconducting
  Electronics (Berlin: De Gruyter)
- [2] Hirschfeld P, Korshunov M and Mazin I 2011 Gap symmetry and structure of Fe-based superconductors *Rep. Prog. Phys.* 74 124508
- [3] Katase T, Ishimaru Y, Tsukamoto A, Hiramatsu H, Kamiya T, Tanabe K and Hosono H 2010 Josephson junction in cobaltdoped BaFe<sub>2</sub>As<sub>2</sub> epitaxial thin films on (La, Sr)(Al, Ta)O<sub>3</sub> bicrystal substrates Appl. Phys. Lett. 96 142507
- [4] Katase T, Ishimaru Y, Tsukamoto A, Hiramatsu H, Kamiya T, Tanabe K and Hosono H 2010 DC superconducting quantum interference devices fabricated using bicrystal grain boundary junctions in Co-doped BaFe<sub>2</sub>As<sub>2</sub> epitaxial films Supercond. Sci. Technol. 23 082001
- [5] Zhang X, Oh Y S, Liu Y, Yan L, Kim K H, Greene R L and Takeuchi I 2009 Observation of the Josephson effect in Pb/Ba<sub>1-x</sub>K<sub>x</sub>Fe<sub>2</sub>As<sub>2</sub> single crystal junctions *Phys. Rev. Lett.* 102 147002
- [6] Reifert D, Hasan N, Döring S, Schmidt S, Monecke M, Feltz M, Schmidl F, Tympel V, Wisniewski W and Mönch I 2014 Preparation of hybrid Josephson junctions on Codoped Ba-122 single crystals Supercond. Sci. Technol. 27 085003
- [7] Kahler D A, Talvacchio J, Murduck J M, Kirschenbaum A, Brooks R, Bu S, Choi J, Kim D M and Eom C-B 2003 Planar Josephson junctions fabricated with magnesium diboride films *IEEE Trans. Appl. Supercond.* 13 1063–6
- [8] Burnell G, Kang D-J, Lee H, Moon S, Oh B and Blamire M 2001 Planar superconductor-normal-superconductor Josephson junctions in MgB<sub>2</sub> Appl. Phys. Lett. 79 3464–6
- [9] Chen K, Cui Y, Li Q and Xi X X 2007 Study of planar MgB<sub>2</sub>/TiB<sub>2</sub>/MgB<sub>2</sub> Josephson junctions using the proximity effect SNS model *IEEE Trans. Appl. Supercond.* 17 955–8

- [10] Lang W and Pedarnig J D 2010 Nanoscience and Engineering in Superconductivity (Berlin: Springer) pp 81–104
- [11] Eisterer M 2017 Radiation effects on iron-based superconductors Supercond. Sci. Technol. 31 013001
- [12] Putti M, Vaglio R and Rowell J 2008 Radiation effects on MgB<sub>2</sub>: a review and a comparison with A15 superconductors Supercond. Sci. Technol. 21 043001
- [13] Withanage W, Kasaei L, Qin F and Xi X X 2019 Aluminum ion implantation in MgB<sub>2</sub> thin films *IEEE Trans. Appl.* Supercond. 29 1–4
- [14] Cybart S A, Cho E, Wong T, Wehlin B H, Ma M K, Huynh C and Dynes R 2015 Nano Josephson superconducting tunnel junctions in  $YBa_2Cu_3O_{7-\delta}$  directly patterned with a focused helium ion beam *Nat. Nanotechnol.* 10 598
- [15] Müller B, Karrer M, Limberger F, Becker M, Schröppel B, Burkhardt C J, Kleiner R, Goldobin E and Koelle D 2019 Josephson junctions and SQUIDs created by focused helium-ion-beam irradiation of YBa<sub>2</sub>Cu<sub>3</sub>O<sub>7</sub> Phys. Rev. Appl. 11 044082
- [16] Kano M, Kohama Y, Graf D, Balakirev F and Sefat A S Mcguire M A, Sales B C, Mandrus D and Tozer S W 2009 Anisotropy of the upper critical field in a Co-doped BaFe<sub>2</sub>As<sub>2</sub> single crystal J. Phys. Soc. Japan 78 084719
- [17] Schilling M B *et al* 2016 Tracing the  $s_{\pm}$  symmetry in iron pnictides by controlled disorder *Phys. Rev.* B **93** 174515
- [18] Gandikota R, Singh R, Kim J, Wilkens B, Newman N, Rowell J, Pogrebnyakov A, Xi X, Redwing J and Xu S 2005 Effect of damage by 2 MeV He ions on the normal and superconducting properties of magnesium diboride *Appl. Phys. Lett.* 86 012508
- [19] Lei Q, Golalikhani M, Yang D, Withanage W, Rafti A, Qiu J, Hambe M, Bauer E, Ronning F and Jia Q 2014 Structural and transport properties of epitaxial Ba(Fe<sub>1-x</sub>Co<sub>x</sub>)<sub>2</sub>As<sub>2</sub> thin films on various substrates Supercond. Sci. Technol. 27 115010
- [20] Xi X X 2009 MgB<sub>2</sub> thin films Supercond. Sci. Technol. 22 043001
- [21] Ziegler J F, Biersack J and Littmark U 1985 *The Stopping and Range of Ions in Matter* vol 1 (New York: Pergamon)
- [22] Kieslich A, Reithmaier J and Forchel A 1994 Minimum feature sizes and ion beam profile for a focused ion beam system with post-objective lens retarding and acceleration mode J. Vac. Sci. Technol. B 12 3518–22
- [23] Lang W, Marksteiner M, Bodea M, Siraj K, Pedarnig J, Kolarova R, Bauer P, Haselgrübler K, Hasenfuss C and

- Beinik I 2012 Ion beam irradiation of cuprate high-temperature superconductors: systematic modification of the electrical properties and fabrication of nanopatterns *Nucl. Instrum. Methods Phys. Res.* B **272** 300–4
- [24] Kasaei L, Melbourne T, Manichev V, Feldman L C, Gustafsson T, Chen K, Xi X X and Davidson B A 2018 MgB<sub>2</sub> Josephson junctions produced by focused helium ion beam irradiation AIP Adv. 8 075020
- [25] Kasaei L, Melbourne T, Li M, Manichev V, Qin F, Hijazi H, Feldman L C, Gustafsson T, Davidson B A, Xi X X and Chen K 2019 Reduced critical current spread in planar Josephson junction MgB<sub>2</sub> array *IEEE Trans. Appl.* Supercond. 29 1–6
- [26] Raineri V, Saggio M and Rimini E 2000 Voids in silicon by He implantation: from basic to applications *J. Mater. Res.* 15 1449–77
- [27] Livengood R, Tan S, Greenzweig Y, Notte J and McVey S 2009 Subsurface damage from helium ions as a function of dose, beam energy, and dose rate J. Vac. Sci. Technol. B 27 3244-9
- [28] Tseng A A 2005 Recent developments in nanofabrication using focused ion beams Small 1 924–39
- [29] Scherzer B M U 1983 Sputtering by Particle Bombardment II ed R Behrisch (Berlin: Springer)
- [30] Park Y-B, Nardi P, Li X and Atwater H A 2005 Nanomechanical characterization of cavity growth and rupture in hydrogen-implanted single-crystal BaTiO<sub>3</sub> J. Appl. Phys. 97 074311
- [31] Leclerc S, Declémy A, Beaufort M, Tromas C and Barbot J 2005 Swelling of SiC under helium implantation J. Appl. Phys. 98 113506
- [32] Wang Y, Kreisel A, Hirschfeld P and Mishra V 2013 Using controlled disorder to distinguish  $s_{\pm}$  and  $s_{++}$  gap structure in Fe-based superconductors *Phys. Rev.* B **87** 094504
- [33] Hirschfeld P J 2016 Using gap symmetry and structure to reveal the pairing mechanism in Fe-based superconductors C. R. Phys. 17 197–231
- [34] Abrikosov A A and Gor'kov L P 1960 Contribution to the theory of superconducting alloys with paramagnetic impurities Zh. Eksp. Teor. Fiz. 39
- [35] Prozorov R, Kończykowski M, Tanatar M A, Thaler A, Bud'ko S L, Canfield P C, Mishra V and Hirschfeld P 2014 Effect of electron irradiation on superconductivity in single crystals of Ba(Fe<sub>1-x</sub>Ru<sub>x</sub>)<sub>2</sub>As<sub>2</sub> (x = 0.24) Phys. Rev. X 4 041032